Colloid and Polymer Science (2021) 299:419–428
https://doi.org/10.1007/s00396-020-04758-6

INVITED ARTICLE

Effect of cosolvent on the rheological properties and self-assembled structures from telechelic polyampholytes

Margarita A. Dyakonova[1] · Yanan Li[1] · Ioanna N. Besiri[2] · Zhenyu Di[3] · Isabelle Grillo[4] · Constantinos Tsitsilianis[2] · Christine M. Papadakis[1]

Received: 30 July 2020 / Revised: 19 September 2020 / Accepted: 25 September 2020 / Published online: 9 October 2020

Abstract

A triblock copolymer with hydrophobic end blocks and a polyampholytic middle block is investigated in a mixture of water and acetone with a focus on the dependence of the rheological properties and of the micellar structure and correlation on the content of acetone. The polymer under study is $PMMA_{86}$-*b*-$P(DEA_{190}$-*co*-$MAA_{96})$-*b*-$PMMA_{86}$, where PMMA stands for poly(methyl methacrylate) and P(DEA-*co*-MAA) for poly(2-(diethylamino) ethyl methacrylate-*co*-methacrylic acid). The pH is chosen at 3. Rheological measurements reveal a transition from a viscoelastic solid over a viscoelastic liquid to a freely flowing liquid upon addition of 5 or 10 wt% of acetone to a 3 wt% aqueous polymer solution, respectively. Using small-angle neutron scattering on 0.5 wt% polymer solutions in water/acetone with the content of the latter ranging between 0 and 30 wt%, significant structural changes are observed as well, such as a decrease of the distance between the PMMA cross-links and of the size of the network clusters upon increasing acetone constant. These changes are attributed to the reduction of the dielectric constant by the addition of the cosolvent acetone, enhancing the flexibility of the middle blocks and their tendency to backfolding, as well as to the decrease of the solvent selectivity, inducing significant exchange rate enhancement of the core-forming PMMA blocks.

Keywords Triblock copolymers · Cosolvent · Rheology · Small-angle neutron scattering

Introduction

Self-assembled hydrogels from telechelic polymers form by hydrophobic interaction, i.e., the hydrophobic end blocks form micelles and a part of the hydrophilic blocks form elastic bridges [1–4]. Using polyelectrolytes as the middle blocks, hydrogels which are responsive to pH and ionic strength have been designed [5–11]. Using a polyampholyte middle block has the advantage of an even stronger pH response. However, non-equilibrium states cannot be excluded especially for long and strongly hydrophobic blocks [4].

We investigated previously a telechelic polyampholyte, namely PMMA-*b*-P(DEA-*co*-MAA)-*b*-PMMA, where PMMA stands for poly(methyl methacrylate) and P(DEA-*co*-MAA) for poly(2-(diethylamino)ethyl methacrylate-*co*-methacrylic acid) [12–14]. While the end blocks are permanently hydrophobic and form "frozen" micelles, the middle block changes from being positively charged at low pH values to being negatively charged at high pH values with an isoelectric point (iep) at pH ~ 8.2. This is reflected both, in the dynamic mechanical properties and the structure of the micellar hydrogel. At pH 3 (the condition chosen in the present work), a freestanding gel is formed at a polymer concentration of 3 wt%. Small-angle neutron scattering (SANS) revealed that, at this pH value, micelles having an average radius of a few nanometer sare formed. Their small size is due to the expanded, strongly charged P(DEA-*co*-MAA) blocks, which only allows for a small aggregation number. The micelles are connected by a low number of stretched P(DEA-*co*-MAA) blocks (bridges) forming loosely packed, large aggregates [12].

This paper is dedicated to the late Isabelle Grillo.

✉ Christine M. Papadakis
papadakis@tum.de

[1] Physik-Department, Fachgebiet Physik weicher Materie, Technische Universität München, James-Franck-Str. 1, 85748 Garching, Germany

[2] Department of Chemical Engineering, University of Patras, 26504 Patras, Greece

[3] Jülich Centre for Neutron Science at MLZ, Forschungszentrum Jülich GmbH, Lichtenbergstr. 1, 85748 Garching, Germany

[4] Large Scale Structures Group, Institut Laue-Langevin, 71, Avenue des Martyrs, 38042 Grenoble, France

In the present work, we alter the nature of the solvent by using water/acetone mixtures. This is expected to have two effects. First, the dielectric permittivity is reduced compared with the one of pure water, which results in an enhanced ion condensation [15]. Second, acetone is a good solvent for PMMA [16] and thus, the mobility of the PMMA end blocks forming the micellar cores is enhanced, while the interfacial tension with water is decreased, enabling the exchange of the PMMA blocks between different micellar cores. Thus, we expect a rearrangement of the network structure, as the acetone content is increased. Besides, acetone is a good solvent for P(DEA-*co*-MAA) [17, 18].

The effect of organic solvent addition on aqueous polymeric systems was addressed previously. Ibraeva et al. studied the effect of addition of ethanol on solution properties of alternating polyampholytes based on *N*,*N*-dimethyldiallylammonium chloride (DM-DAAC) and alkyl (aryl) substituted maleamic acids in water-ethanol mixtures containing 0.15 M KCl [19]. The authors observed that the viscosity, which was low in an aqueous solution containing salt, gradually increased upon addition of ethanol. The underlying change of the conformation of the polymer chains from compact in ethanol-free solutions to expanded in water-ethanol mixtures was attributed to the preferential solvation of both polymer segments. The ionic and hydrophilic segments interact with the polar solvent, i.e., water, whereas the hydrophobic segments interact with the organic solvent.

Tsitsilianis et al. investigated the effect of addition of dimethylformamide (DMF) on the rheological properties of a reversible hydrogel from the telechelic polyelectrolyte polystyrene-*b*-poly(acrylic acid)-*b*-polystyrene (PS-*b*-PAA-*b*-PS) [20]. A transition from a concentrated suspension of swollen polyelectrolyte clusters (microgels) to a more homogeneous, kinetically controlled 3D network was observed. This structural rearrangement was assigned to a two-fold effect of DMF. Firstly, it lowers the dielectric permittivity of the medium, and, hence, increases the flexibility of the elastically active PAA chains. Secondly, being a good solvent for the PS blocks, DMF increases their mobility, which enhances the exchange rate of solvated PS stickers between the physical cross-links.

The effect of addition of methanol on the structure and rheological properties of hydrogels from a pentablock terpolymer PMMA-*b*-PAA-*b*-P2VP-*b*-PAA-*b*-PMMA, comprising the polyampholytic triblock copolymer PAA-*b*-P2VP-*b*-PAA and hydrophobic PMMA end blocks, was studied by Tsitsilianis et al. [21]. The authors observed a sol-gel-sol transition in the high pH regime, induced by varying the methanol/H_2O ratio. They explained this effect by the opposite solubility effect of MeOH on the two blocks of the elastically active chains, namely, PAA and P2VP. On the one hand, MeOH increases the solubility of the P2VP segments which, at high pH values, are non-ionized. On the other hand, MeOH reduces the dielectric permittivity of the medium and thus lowers the degree of ionization of the PAA segments due to enhanced ion condensation. Thus, the interplay between the hydrophobic and electrostatic interactions defines the resulting polymer behavior in solution.

We investigate here $PMMA_{86}$-*b*-P(DEA_{190}-*co*-MAA_{96})-*b*-$PMMA_{86}$ in mixtures of D_2O and $(CD_3)_2CO$ of varying composition at pH 3. At this pH value, a freestanding gel was observed in pure D_2O for a polymer concentration of 3 wt% [13]. It consists of network clusters with the cross-links being formed by PMMA, which are connected by expanded P(DEA-*co*-MAA) blocks [13]. A similar micellar structure was obtained at a much lower polymer concentrations (0.05 wt%, [14]). Rheological measurements on solutions having a polymer concentration of 3 wt% indicate strong changes of the mechanical properties upon addition of small amounts of acetone. To investigate the mesoscopic structures, we use SANS on solutions with polymer concentrations of 0.5 wt% prepared in predeuterated solvents. This lower polymer concentration is chosen so equilibrium can be installed, while at the same time, decent scattering intensities can be obtained. For the sample preparation, we chose two methods, i.e., (i) addition of polymer to the solvent mixture (method I) and (ii) dissolution of the polymer in $(CD_3)_2CO$, partial evaporation of $(CD_3)_2CO$, and subsequent addition of D_2O (method II). In the former case, both solvents are present at once, whereas in the latter case, the PMMA blocks are presumably fully dissolved in $(CD_3)_2CO$ and form micelles only upon addition of D_2O.

Materials and methods

Materials

The sample under study is the triblock terpolymer poly(methyl methacrylate)-*b*-poly(2-(diethylamino)ethyl methacrylate-*co*-methacrylic acid)-*b*-poly(methyl methacrylate), $PMMA_{86}$-*b*-P(DEA_{190}-*co*-MAA_{96})-*b*-$PMMA_{86}$. Its molar mass is $M_w = 60{,}100$ g mol^{-1} and its dispersity $Đ = 1.30$ [13]. The details of the synthesis are given elsewhere [13]. For SANS investigations, D_2O and $(CD_3)_2CO$ (both from Deutero GmbH, Kastellaun, Germany) were used as solvents. The dielectric constants of D_2O and $(CD_3)_2CO$ at room temperature are $\varepsilon_r = 78.1$ [22] and 20.7 [23], respectively, leading to dielectric constants of the $D_2O/(CD_3)_2CO$ mixtures between 78.1 and ~ 61 for fractions of $(CD_3)_2CO$ between 0 and 30 wt%.

Samples for rheology were prepared by adding acetone to 3 wt% polymer solutions in H_2O. All samples were prepared following the same protocol. In detail, $PMMA_{86}$-*b*-P(DEA_{190}-*co*-MAA_{96})-*b*-$PMMA_{86}$ was dispersed in low pH distilled water, controlled by HCl. Then, the samples were

homogenized using a Sigma 2K15 centrifugator with 3500 rpm/min at 20 °C for several hours. Finally, 5 or 10 wt% acetone was added, and the samples were again homogenized. In all cases, the pH value was adjusted at a value 3 by addition of 0.1 M HCl.

Samples for SANS were prepared in two ways. In method I, pre-weighed amounts of $PMMA_{86}$-*b*-P(DEA_{190}-*co*-MAA_{96})-*b*-$PMMA_{86}$ were dissolved in D_2O/$(CD_3)_2CO$ mixtures at room temperature to achieve a polymer concentration of 0.5 wt%. These solutions were stirred for 24 h at 26 °C, taking care to prevent the evaporation of $(CD_3)_2CO$. The pH value was found at 3.4–3.6. A small drop of 0.1 M hydrochloric acid (HCl) in D_2O was added, and the solution was stirred for 1 h at 26 °C. This step was repeated until the pH had reached a value of 3.0. The solutions were left to shake overnight and were then centrifuged at 3000 rpm for 15 min. For $(CD_3)_2CO$ contents below 15 wt%, the solutions were once more shaken and were centrifuged again. In all cases, complete dissolution of polymer was achieved by centrifuging several times, also with the bottle placed upside down. The pH was tested once more. In most cases, the pH was slightly higher than 3.0; therefore, more acid was added, and the sample was shaken and centrifuged once more. Samples containing up to 15 wt% of $(CD_3)_2CO$ were slightly turbid, whereas those with higher contents were transparent. Samples containing 0–10 wt% of $(CD_3)_2CO$ were gels, whereas those with 15–30 wt% were liquids.

In method II, the polymers were dissolved in $(CD_3)_2CO$ at room temperature. The solution was stirred for 24 h at 26 °C and was subsequently centrifuged at 3000 rpm for 15 min, also with the bottle placed upside down. This procedure was repeated several times, and the samples were left to shake for at least 2 desired amount of $(CD_3)_2CO$ in the sample was achieved by letting the superfluous acetone evaporate. Afterwards, a calculated amount of D_2O was added to install the desired concentration of polymer of 0.5 wt%. The pH value was adjusted at 3.0 by adding 0.1 M hydrochloric acid (HCl) in D_2O. The gels were again homogenized by stirring and centrifuging. Samples containing 0–10 wt% of $(CD_3)_2CO$ were gels, whereas those with 15–30 wt% were liquids. The fraction of $(CD_3)_2CO$ was chosen at values between 0 and 30 wt%.

Methods

Rheology

Rheological measurements were conducted using a stress rheometer (AR-2000ex, TA instruments) with a cone-and-plate geometry (20 mm, 4° angle). All experiments were conducted at 25 °C.

Small-angle neutron scattering

SANS measurements on the samples prepared by method I were carried out at the instrument KWS-1 (JCNS at the Maier-Leibnitz-Zentrum (MLZ) in Garching, Germany) [24, 25]. The neutron wavelength was chosen at $\lambda = 0.47$ nm with a spread $\Delta\lambda/\lambda = 20\%$. Using sample-detector distances (SDDs) of 1.17 m, 7.67 m, and 19.67 m, a range of momentum transfers $q = 0.026$ to 4.6 nm^{-1} was covered. $q = 4\pi \times \sin(\theta/2)/\lambda$ where θ is the scattering angle. The exposure times were 10, 25, and 45 min at SDD = 1.17 m, 7.67 m, and 19.67 m, respectively. The samples were mounted in 1 mm quartz glass cuvettes (Hellma) and were measured at room temperature. Boron carbide was used for measurement of the dark current. Poly(methyl methacrylate) was used to measure the detector sensitivity and for calibration of the intensity. The scattering of the D_2O filled cell was subtracted from the sample scattering, taking the transmissions into account. The data were azimuthally averaged. All data reductions were performed with the software QtiKWS provided by JCNS.

SANS measurements on the samples prepared by method II were carried out at the instrument D33 at the Institut Laue-Langevin (ILL) in Grenoble, France. The neutron wavelength was chosen at $\lambda = 0.5$ nm with a spread $\Delta\lambda/\lambda = 10\%$. The scattering signal was collected by a 128×1288 ^{3}He tube detector having a pixel size of 0.5×0.5 cm^2. Using SDDs of 2 m and additionally 12.8 m, a range of momentum transfers $q = 0.036$ to 5.7 nm^{-1} was covered. Some samples were additionally measured at a SDD of 12.5 m with $\lambda = 1.0$ nm, which enlarges the q range to 0.024 to 5.7 nm^{-1}. The samples with $(CD_3)_2CO$ contents from 0 to 10 wt% were mounted in 1 mm quartz cuvettes (Hellma), whereas the samples with $(CD_3)_2CO$ contents of 15–30 wt% were mounted in 2 mm quartz cuvettes (Hellma). All samples were measured at room temperature. The exposure times were 15 min and 30 min at SDD = 2 m and 12.5 m ($\lambda = 0.5$ nm) and 55 min for 12.5 m and $\lambda = 1.0$ nm, respectively. Boron carbide was used to determine the dark current. For detector sensitivity measurements and for bringing the data to absolute scale, H_2O was used. The scattering of the empty cell was subtracted from the sample scattering, taking the transmissions into account. The data were azimuthally averaged. Data reduction was performed using the software LAMP provided by ILL.

SANS data analysis

For fitting of the SANS curves, the following fitting function was used:

$$I(q) = I_{ls}(q) + P_{sph}(q)S_{HS}(q) + I_{fluct}(q) + I_{bg} \quad (1)$$

where $I_{ls}(q)$ denotes scattering from large-scale structures. $P_{sph}(q)$ denotes the form factor of spheres, formed by PMMA, and $S_{HS}(q)$ denotes the structure factor

describing their correlation. $I_{\mathrm{fluct}}(q)$ denotes concentration fluctuations on small length scales, mainly by the P(DEA$_{190}$-*co*-MAA$_{96}$) midblocks forming the matrix between the PMMA-rich spheres. I_{bg} denotes the incoherent background.

For $I_{\mathrm{ls}}(q)$, a modified Porod law was used [26]:

$$I_{ls}(q) = \frac{I_{P,0}}{q^{\alpha}}, \tag{2}$$

where $I_{P,0}$ is a scaling factor and α is the Porod exponent of the large-scale structures. The values of the exponent α characterize the surface roughness of the aggregates at large length scales [27].

The form factor of sphere form factor was used [28]:

$$P_{\mathrm{sph}}(q,r) = \frac{I_{\mathrm{sph},0}}{V}\left[\frac{3V(\Delta\rho)(\sin(qr)-qr\cos(qr))}{(qr)^3}\right]^2 \tag{3}$$

where $I_{\mathrm{sph},0}$ is the scaling factor, V is the sphere volume, $\Delta\rho$ is the difference of scattering length densities (SLDs) of the sphere and the surrounding, and r is the radius of the spheres. The SLD values of the solvent mixture was calculated as a weighted average of the values for D_2O, 6.36×10^{10} cm^{-2}, and $(CD_3)_2CO$, 5.35×10^{10} cm^{-2} [29]. The SLD value of the spheres was treated as a floating parameter. The distribution of r was accounted for by the following integration [30]:

$$P_{\mathrm{cs}}(q) = \frac{1}{V_{\mathrm{mic}}}\int_0^{\infty} f(r)P_{\mathrm{sph}}(q,r)dr \tag{4}$$

where $f(r)$ is the normalized Schulz distribution [31].

$$f(r) = (z+1)^{z+1}\, u^2\, \frac{u\exp[-(z+1)u]}{\sigma\,\Gamma(z+1)} \tag{5}$$

$u = r/R$, where R is the average sphere radius, and z is related to the polydispersity by $z = 1/(p^2-1)$. $p = \sigma/R$, and σ^2 is the variance of the distribution. In most cases, p was 0.5.

To describe the interparticle interactions, the Percus-Yevick hard-sphere structure factor $S_{HS}(q)$ was used [32]:

$$S_{\mathrm{HS}}(q) = \frac{1}{1+24\eta G(2R_{\mathrm{HS}}q)/(2R_{\mathrm{HS}}q)}, \tag{6}$$

where R_{HS} denotes the hard-sphere radius, or half the average distance between the centers of correlated particles, and η denotes the volume fraction of correlated micelles. The function $G(x)$ is given by:

$$G(x) = \gamma\frac{\sin x - x\cos x}{x^2} + \delta\frac{2x\sin x + (2-x^2)\cos x - 2}{x^3} + \varepsilon\frac{-x^4\cos x + 4(3x^2 - 6\cos x + (x^3-6x)\sin x + 6)}{x^5} \tag{7}$$

with the parameters

$$\gamma = \frac{(1+2\eta)^2}{(1-\eta)^4}; \delta = \frac{-6\eta(1+\eta/2)^2}{(1-\eta)^4}; \varepsilon = \frac{\gamma\eta}{2} \tag{8}$$

The local concentration fluctuations, mainly due to the P(DEA$_{190}$-*co*-MAA$_{96}$) blocks in the shell and the matrix, are modeled using the Ornstein-Zernike structure factor:

$$I_{\mathrm{fluct}}(q) = \frac{I_{OZ}}{1+q^2\xi^2} \tag{9}$$

where I_{OZ} is the amplitude and ξ, is the correlation length. Fitting was carried out using the software SASView 4.2.2 [33]. At this, the resolution function was taken into account.

Results

In this section, we first present and discuss preliminary results obtained from rheology. Then, SANS results on samples prepared by the two methods described in the "Introduction" section are presented. Finally, we compare the results and draw conclusions on the effect of the cosolvent on the network structure.

Rheological results

The addition of 5 or 10 wt% of acetone has a strong effect on the macroscopic flow properties of a 3 wt% solution of PMMA$_{86}$-*b*-P(DEA$_{190}$-*co*-MAA$_{96}$)-*b*-PMMA$_{86}$ in H_2O at pH 3 (Fig. 1). While the sample in pure H_2O is a freestanding gel, in accordance with our previous investigations [13], it becomes a viscoelastic liquid after addition of 5 wt% of acetone and flows after addition of 10 wt% of acetone.

In Fig. 2 a and b, rheological results are presented, namely, the shear viscosity versus the shear rate for a 3 wt% polymer solution at pH 3 in pure water and with 5 wt% of acetone. As seen, by just adding 5 wt% of acetone, the viscosity decreases by about two orders of magnitudes at all shear rates applied (Fig. 2a). In agreement with the usual behavior of telechelic associative gelators, no Newtonian plateau can be observed at low shear, neither in pure water nor in water/acetone.

Moreover, from the creep experiments, the compliance $J(t)$ is obtained which reaches a linear region with a constant deformation rate almost after 450 s of the measurements (Fig. 2b). From the relationship $J(t) = J_o + t/\eta_0$, we can estimate the zero shear viscosity, the compliance in the plateau region, J_o, and the terminal relaxation time of the network, given by the equations $J_o = G_0^{-1}$ and $\tau_R = \eta_0/G_0$, respectively (Table 1). It is seen that $J(t)$ strongly depends on the presence of the organic solvent. While the polymer dissolved in pure water behaves like a viscoelastic solid (freestanding gel), for 5 wt%

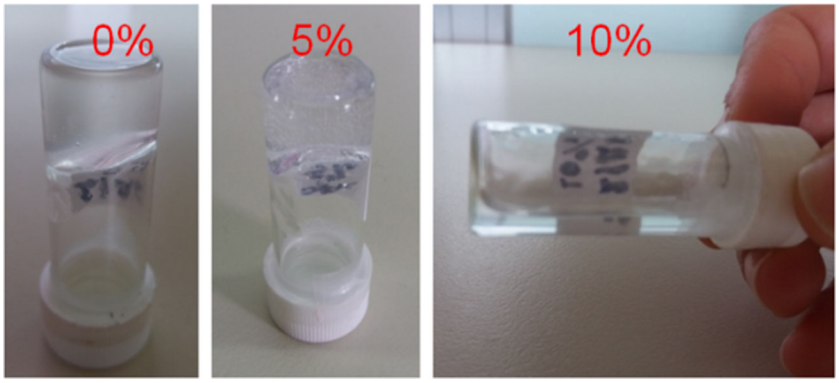

Fig. 1 Macroscopic images of 3 wt% $PMMA_{86}$-*b*-P(DEA_{190}-*co*-MAA_{96})-*b*-$PMMA_{86}$ solutions in H_2O at pH 3 at different concentrations of acetone, as depicted with red letters

acetone, the hydrogel loses much elasticity and behaves like a viscoelastic liquid. Importantly, acetone causes a substantial decrease of τ_R by about one order of magnitude, which in turn, affects the zero shear viscosity. Moreover, the elasticity of the system is decreased at 5 wt% of acetone, and it vanishes at 10 wt%, resulting in a freely flowing liquid (Fig. 1).

The lower relaxation time in the presence of acetone indicates that the exchange dynamics of the network is enhanced. As is well known, the terminal relaxation time of networks, formed in selective solvents by physically cross-linked triblock copolymers with associative end blocks, depends on the exchange kinetics of the core-forming blocks (physical cross-links). These cores are formed because of the unfavorable interactions between the end blocks and the solvent (selective media), which are reflected in the Flory-Huggins interaction parameter χ. The relaxation time is related to the energy barrier that has to be overcome for a core-forming block to escape from its core. This barrier is proportional to $N^{2/3}\ \gamma$, where N is the degree of polymerization of the end block and γ is the surface tension of the core with respect to the solvent, which, in turn, is related to the χ parameter [34]. Recently, Lodge et al. quantified the role of χ in chain exchange kinetics of block copolymer micelles in binary solvent mixtures [35, 36]. By exploring the influence of solvent composition on the chain exchange kinetics between micelles, a dramatic acceleration of the exchange rate was found. The rate increased by about 5 orders of magnitude, when just 25 vol% of good solvent for the core-forming block were added to the solvent mixture, imposing a decrease of the χ parameter [36]. In the present case, the addition of 5 wt% acetone reduces χ as well, which reduces γ and hence increases the exchange rate of the stickers by about an order of magnitude, as reflected in the decrease of the relaxation time. Even faster exchange kinetics are observed at 10 wt% acetone, when the relaxation time is unmeasurably low (freely flowing liquid). Our results in aqueous media are in good agreement with the hypersensitivity of the exchange rate to the Flory-Huggins interaction parameter χ (solvent selectivity), as theoretically predicted and experimentally observed in other micellar systems in organic solvents [36] and ionic liquids [35].

In pure water, a kinetically "frozen" hydrogel (out of equilibrium) is formed, and its rheological characteristics depend strongly on the preparation conditions. By adding acetone, the selectivity of the solvent is decreased, and the hydrogel is transformed into a viscoelastic system with detectable exchange kinetics. Based on the above findings, we tried to prepare a 3 wt% aqueous polymer solution in the presence

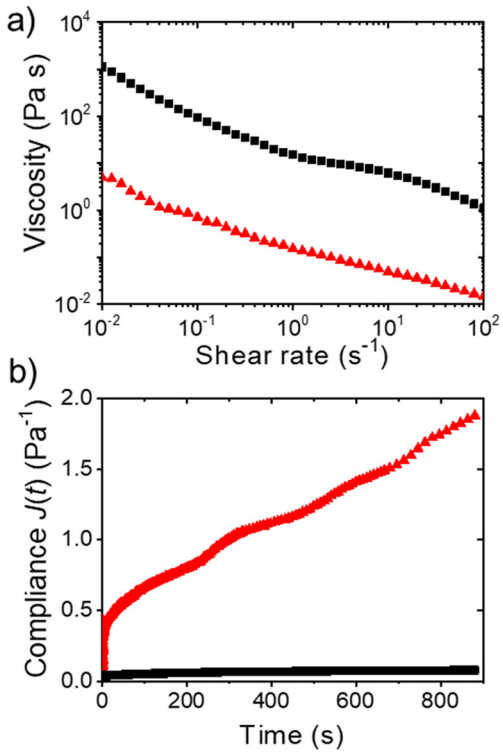

Fig. 2 Rheological data from a 3 wt% solution of $PMMA_{86}$-*b*-P(DEA_{190}-*co*-MAA_{96})-*b*-$PMMA_{86}$ in pure H_2O (black squares) and in a mixture of H_2O with 5 wt% of $(CH_3)_2CO$ (red triangles). **a** Viscosity in dependence on the shear rate. **b** Time evolution of the compliance in presence (applied shear stress, $\sigma = 0.05$ Pa) and absence ($\sigma = 0.5$ Pa) of 5 wt% of acetone

Table 1 Data from creep experiments for 3 wt% polymer hydrogels

Acetone content (wt%)	G_o (Pa)	η_o (Pa s)	τ_R (s)
0	17.43	49.5×10^3	2840
5	2.36	613.5	260

of 10 wt% of acetone in order to detect a possible improvement of the network structure. First, we added the polymer to water in the presence of HCl and acetone. The sample was homogenized, and subsequently, the solution was placed in the oven at 40 °C for the evaporation of acetone. Finally, distilled water was added to the solution to adjust the 3 wt% polymer concentration, and the gel was again homogenized. After removing the acetone by evaporation, an oscillatory shear experiment was conducted. The storage modulus was found to be increased by about one order of magnitude with respect to the hydrogel formed directly in water [13] without the aid of acetone (Fig. 3). Thus, a rearrangement of the network structure was achieved, due to the enhanced mobility of the PMMA end blocks, which leads to an increase of the number of bridging chains, as reflected in the enhanced elasticity of the network.

Obviously, the preparation method affects the underlying structure of the gel. This motivated us for a more systematic investigation of the influence of acetone and the preparation method on the micellar structure using SANS.

Structural changes as revealed by SANS

The SANS data of solutions of $PMMA_{86}$-*b*-P(DEA_{190}-*co*-MAA_{96})-*b*-$PMMA_{86}$ at 0.5 wt% in D_2O/$(CD_3)_2CO$ mixtures with varying $(CD_3)_2CO$ content prepared by method I (i.e., dissolution of the polymer in the D_2O/$(CD_3)_2CO$ mixtures) are presented in Fig. 4. The curve of the solution in pure D_2O and the ones of solutions with $(CD_3)_2CO$ contents in the solvent mixture up to 10 wt% have a similar shape, namely, a shallow maximum at ~0.12–0.13 nm^{-1}. In contrast, the curves between 15 and 25 wt% feature forward scattering, which ranges up to ~0.06 nm^{-1} at 15 wt% and up to 0.09 nm^{-1} at 25 wt%, i.e., it moves to higher q values. It may be attributed to large clusters of micelles. Moreover, the above mentioned maximum becomes more pronounced and is now located at $q = 0.13$–0.14 nm^{-1}. The scattering at q values higher than the maximum has a

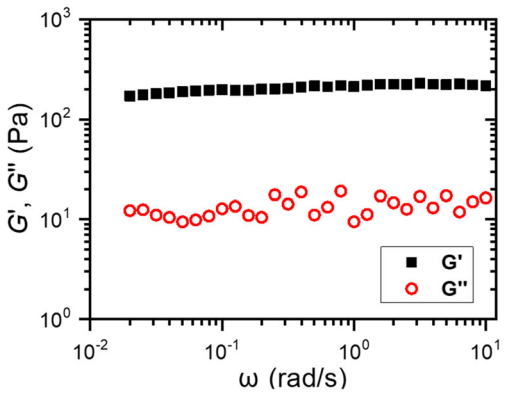

Fig. 3 Viscoelastic parameters of 3 wt% $PMMA_{86}$-*b*-P(DEA_{190}-*co*-MAA_{96})-*b*-$PMMA_{86}$ solutions prepared with the evaporation of 10 wt% acetone as a function of angular frequency. The strain amplitude was 0.1%

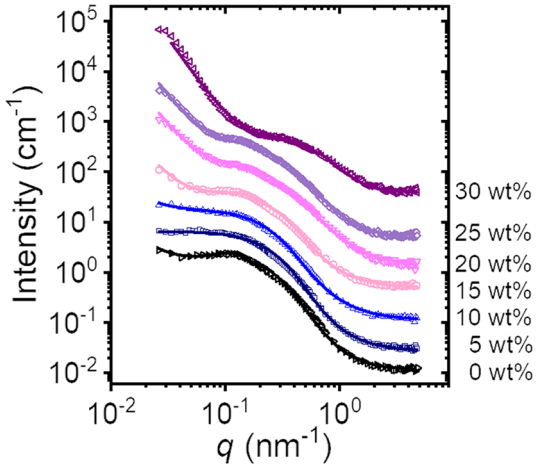

Fig. 4 SANS curves of 0.5 wt% $PMMA_{86}$-*b*-P(DEA_{190}-*co*-MAA_{96})-*b*-$PMMA_{86}$ solutions at 26 °C at pH 3.0 in mixtures of D_2O/$(CD_3)_2CO$ prepared by method I. The weight fractions of $(CD_3)_2CO$ in the solvent mixture are indicated in the graph. The symbols represent the data, and the solid lines represent the model fits. The curves are shifted vertically by factors of 3 with respect to each other (5–25 wt%) and 6 (25 and 30 wt%)

different shape than at lower $(CD_3)_2CO$ contents, and this "shoulder" moves to higher q values. At 30 wt% of $(CD_3)_2CO$, the curve shape is significantly different. Strong and steep forward scattering extends to ~0.18 nm^{-1}, the maximum is very weak and shifted to 0.35 nm^{-1}, and a broad shoulder extends to high q values (up to ~2.3 nm^{-1}).

We first discuss the results of the solution in pure D_2O. The scattering curve was fitted using Eq. 1, and good agreement is achieved. Possibly, better fits might have been obtained with more complex models, such as those used in our previous studies [14]; however, these would imply a higher number of fitting parameters, making the results more ambiguous. The resulting average radius of the spheres, deduced from the form factor of polydisperse spheres (Eq. 3) is $R = 2.61 \pm 0.02$ nm (Fig. 5a). This value is similar to the one obtained by us earlier for polymer concentrations of 0.05 and 3.0 wt% [14]. We assume that the particles correspond to the PMMA cores along with the inner dense part of the shell formed by the middle blocks. From fitting of the Percus-Yevick structure factor (Eqs. 6–8), we derive the value of the hard-sphere radius at $R_{HS} = 24.2$ nm (Fig. 5a), which corresponds to half the distance between the correlated micelles. The half-distance is thus significantly larger than the average micellar radius. At the pH value chosen, a large fraction of DEA segments is protonated, which leads to repulsive electrostatic interactions between similarly charged units along the polyampholyte middle block. As a result, the middle block adopts a stretched conformation and can bridge distant neighboring micelles. The hard-sphere volume fraction is found at $\eta_{HS} = 0.1$ (Fig. 5b), thus the spheres are weakly correlated with each other. This morphology is consistent with the viscoelastic appearance of the sample. The correlation length ξ is found at 7 nm, which reflects the concentration fluctuations of the middle polyampholyte blocks between the PMMA spheres.

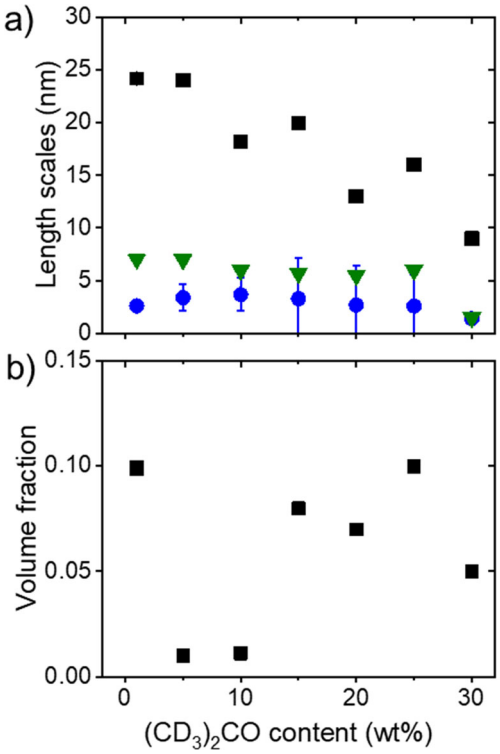

Fig. 5 Parameters from fitting of the SANS curves in Fig. 4. (a) Blue circles, average sphere radius R; black squares, hard-sphere radius R_{HS}; green triangles down, correlation length ξ. (b) Volume fraction of correlated spheres, η

With the $(CD_3)_2CO$ content in the solvent mixture increasing to 25 wt%, the sphere radius and the correlation length are rather unchanged, but the distance between the spheres decreases steadily to 16 nm at 25 wt%. At 5 and 10 wt%, the volume fraction of correlated micelles is low, but scatters around 0.07 and 0.1 at 15–25 wt%. (The uncertainties of this parameter are rather high.) At 5–10 wt%, $(CD_3)_2CO$ lowers the dielectric permittivity of the medium by 5–6 units; thus, due to ion condensation, the strength of the repulsive electrostatic interactions between the charged DEA units in the bridging polyampholytic blocks is slightly reduced. As a consequence, the middle blocks are more flexible than in pure D_2O. The slight increase of forward scattering indicates that the micellar clusters break up in consistency with the rheological findings (Fig. 3). At 15–25 wt%, the correlation between the micelles within the clusters becomes stronger, but the strong forward scattering at low q values ($q < 0.06$–0.09 nm^{-1}) shows that the micellar clusters are of finite size. Presumably, the larger clusters in pure D_2O or lower $(CD_3)_2CO$ contents are disrupted, when the middle blocks become more flexible, enabling a bridge-to-loop transition. This is consistent with the liquid appearance of the samples. The Porod exponent increases from 2.85 at 10 wt% of $(CD_3)_2CO$ to 3.15 at 30 wt%, i.e., the clusters become more compact.

Significant differences are observed at 30 wt% of $(CD_3)_2CO$ (Fig. 4). The structure factor peak is much weaker than at lower $(CD_3)_2CO$ contents, and forward scattering is strong and extends to higher q values (up to ~ 0.18 nm^{-1}). The average sphere radius has decreased to $R = 1.4$ nm, suggesting that the micelles are now very small and consist of very few PMMA end blocks, i.e., the micellar network has transformed into clusters of random networks. These clusters are smaller than at lower $(CD_3)_2CO$ contents. The correlation length and the hard-sphere radius have also decreased significantly. We suppose, that at this relatively high concentration of $(CD_3)_2CO$, the selectivity of the solvent has been significantly reduced, resulting in a weak association of the PMMA blocks and hence in very low aggregation numbers. Moreover, the lower dielectric permittivity of the medium promotes the flexibility of the P(DEA$_{190}$-*co*-MAA$_{96}$) polyelectrolyte chains due to ion condensation, facilitating backfolding. Both effects lead to small micelles and small clusters.

The question arises whether the samples described above are in equilibrium. Therefore, we chose an alternative preparation method which targets the initial dissolution of the PMMA end blocks in $(CD_3)_2CO$ and the subsequent micelle formation by addition of D_2O (method II). The SANS data are shown in Fig. 6. Interestingly, already for the lowest $(CD_3)_2CO$ contents, forward scattering is observed, which becomes steeper with increasing content. As the $(CD_3)_2CO$ content in the solvent mixture is increased to 7 wt%, the maximum becomes shallower. At 15–30 wt%, the forward scattering extends to higher q values, the maximum is at a higher q value (~ 0.28 nm^{-1}), and a second shoulder appears. These curves are fitted with the same model as before (Eqs. 1–9). Again, good fits are obtained (Fig. 6).

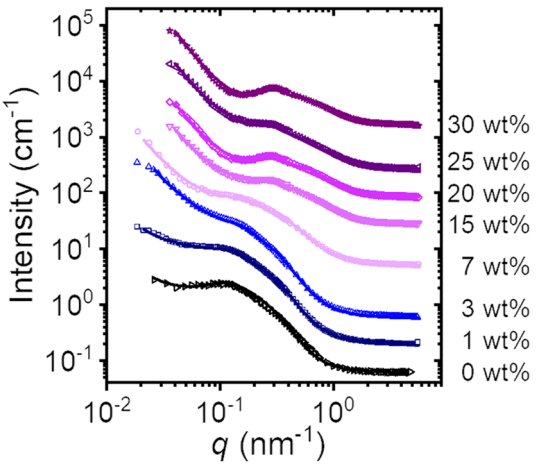

Fig. 6 SANS curves of 0.5 wt% PMMA$_{86}$-*b*-P(DEA$_{190}$-*co*-MAA$_{96}$)-*b*-PMMA$_{86}$ solutions at 26 °C at pH 3.0 in mixtures of $D_2O/(CD_3)_2CO$, prepared by method II. The weight fractions of $(CD_3)_2CO$ in the solvent mixture are indicated in the graph. The symbols represent the data, and the solid lines the model fits. The curves are shifted vertically by factors of 3 with respect to each other, except the data at 7, 15, and 30 wt%, which were shifted by factors of 9, 6, and 6, respectively. The minimum value of q is lower at 1–7 wt%, because in these cases, an additional setting was used. The data from the solution in pure D_2O from Fig. 1 are added (a constant of 0.05 cm^{-1} was added to the intensities to compensate for the difference in incoherent background)

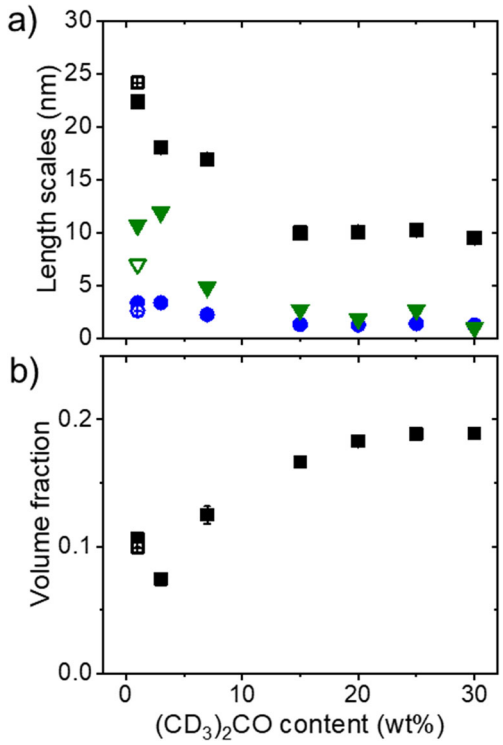

Fig. 7 Parameters from fitting of the SANS curves in Fig. 6 (closed symbols) and from the one in pure D_2O from Fig. 4. (a) Blue circles, average sphere radius R; black squares, hard-sphere radius R_{HS}; green triangles down, correlation length ξ. (b) Volume fraction of correlated spheres, η

The resulting fitting parameters are shown in Fig. 7. Between 1 and 15 wt% of $(CD_3)_2CO$, the radius of the spheres decreases, i.e., the aggregation number decreases (Fig. 7a). In this range, the hard-sphere radius decreases as well, and the volume fraction increases from 0.1 to 0.2 (Fig. 7b). Thus, the distance between the correlated micelles decreases, and the volume fraction of the correlated micelles increases. The correlation length ξ decreases from 7.0 to 2.7 nm (Fig. 7a). The Porod exponent which characterizes the clusters of micelles, increases from ca. 2.5 to 2.8 (not shown), indicating loosely packed clusters of micelles.

In the range 20–30 wt%, all parameters stay rather constant. Only, the correlation length decreases from 1.8–2.7 nm at 15–25 wt% to 1.0 nm at 30 wt% of $(CD_3)_2CO$ in the solvent mixture, i.e., the chains become more densely packed, which may reflect their increasing flexibility.

Comparing these values with the ones from preparation method I in pure D_2O (Fig. 5), it is seen that the sphere radii are rather similar. For method I, the hard-sphere radius is throughout larger, and the volume fraction of correlated micelles is smaller than with method II. The forward scattering is less pronounced in the SANS curves from the samples prepared by method I, i.e., the network clusters are more extended. Thus, while both sample series overall show the same trends upon addition of $(CD_3)_2CO$, the sample preparation method seems to play a certain role.

Conclusion

The effect of addition of acetone on the rheological and structural properties of a micellar network from the telechelic polyampholyte PMMA-*b*-P(DEA-*co*-MAA)-*b*-PMMA in aqueous solution at pH 3 was studied in a wide range of acetone concentrations. Rheology on 3 wt% solutions of the polymer in water revealed a transition from a freestanding gel over a viscoelastic liquid to a viscous liquid, as 5 and 10 wt% of acetone were added. SANS on a 0.5 wt% solution in pure water reveals clusters from spherical micelles formed by (presumably) glassy PMMA blocks, which are bridged by strongly stretched polyampholytic middle blocks. The addition of acetone has a strong influence on the network architecture, which is assigned to its twofold effect. Firstly, it decreases the dielectric constant of the solvent, which reduces the effective charge density on the polyampholytic middle blocks. This results in a higher flexibility of the middle blocks and reduces the distance between the micelles and the size of the network clusters. Secondly, and more importantly, being a good solvent for PMMA, $(CD_3)_2CO$ alters dramatically the exchange dynamics of PMMA stickers between the different hydrophobic physical cross-links in the network, inducing also lower aggregation numbers, due to the reduction of the solvent selectivity. The second effect dominates the rheological properties. While altering the sample preparation method results in quantitative differences, SANS gives detailed information about the effects of the cosolvent on a wide range of length scales. Addition of a cosolvent is thus, apart from changes of the pH and the ionic strength, another route for the manipulation of the network architecture and thus the mechanical properties.

Acknowledgments We thank K. Kyriakos, B.-J. Niebuur, K. N. Raftopoulos, and N. S. Vishnevetskaya (all at Technical University of Munich) for helping with the experiments. This work is based upon the experiments performed at the KWS-1 instrument operated by the JCNS at the Heinz Maier-Leibnitz Zentrum (MLZ), Garching, Germany. We acknowledge beam time allocation and excellent equipment. We acknowledge ILL for the allocation of beam time at instrument D33 and excellent equipment (DOI:https://doi.org/10.5291/ILL-DATA.9-11-1734).

Funding Open Access funding enabled and organized by Projekt DEAL.

Compliance with ethical standards

Conflict of interest The authors declare that they have no conflict of interest.

References

1. Winnik MA, Yekta A (1997) Associative polymers in aqueous solution. Curr Opin Colloid Interface Sci 2:424–436. https://doi.org/10.1016/S1359-0294(97)80088-X
2. Berret J-F, Calvet D, Collet A, Viguier M (2003) Fluorocarbon associative polymers. Curr Opin Colloid Interface Sci 8:296–306. https://doi.org/10.1016/S1359-0294(03)00048-7
3. Xu C, Kopeček J (2007) Self-assembling hydrogels. Polym Bull 58:53–63. https://doi.org/10.1007/s00289-006-0597-0
4. Chassenieux C, Nicolai T, Benyahia L (2011) Rheology of associative polymer solutions. Curr Opin Colloid Polym Sci 16:18–26. https://doi.org/10.1016/j.cocis.2010.07.007
5. Kimerling AS, Rochefort WES, Bhatia SR (2006) Rheology of block polyelectrolyte solutions and gels: a review. Ind Eng Chem Res 45:6885–6889. https://doi.org/10.1021/ie051034o
6. Bossard F, Aubry T, Gotzamanis G, Tsitsilianis C (2006) pH-tunable rheological properties of a telechelic cationic polyelectrolyte reversible hydrogel. Soft Matter 2:510–516. https://doi.org/10.1039/b601435f
7. Kopeček J, Yang Y (2007) Hydrogels as smart biomaterials. Polym Int 56:1078–1098. https://doi.org/10.1002/pi.2253
8. Ahn S-K, Kasi RM, Kim S-C, Sharma N, Zhou Y (2008) Stimuli-responsive polymer gels. Soft Matter 4:1151–1157. https://doi.org/10.1039/b714376a
9. Tsitsilianis C (2010) Responsive reversible hydrogels from associative "smart" macromolecules. Soft Matter 6:2372–2388. https://doi.org/10.1039/b923947
10. Zhang R, Shi T, An L, Huang Q (2011) Salt effects on sol-gel transition of telechelic polyelectrolytes in aqueous solutions. Macromolecules 45:555–562. https://doi.org/10.1021/ma201872e
11. Madsen J, Armes SP (2012) (Meth)acrylic stimulus-responsive block copolymer hydrogels. Soft Matter 8:592–605. https://doi.org/10.1039/c1sm06035j
12. Tsitsilianis C, Gotzamanis G, Iatridi S (2011) Design of "smart" segmented polymers by incorporating random copolymers as building blocks. Eur Polym J 47:597–510. https://doi.org/10.1016/j.eurpolymj.2010.10.005
13. Gotzamanis G, Papadimitriou K, Tsitsilianis C (2016) Design of a C-*b*-(A-*co*-B)-*b*-C telechelic polyampholyte pH-responsive gelator. Polym Chem 7:2121–2129. https://doi.org/10.1039/C5PY02066B
14. Dyakonova MA, Gotzamanis G, Niebuur B-J, Vishnevetskaya NS, Raftopoulos KN, Di Z, Filippov SK, Tsitsilianis C, Papadakis CM (2017) pH responsiveness of hydrogels formed by telechelic polyampholytes. Soft Matter 13:3568–3579. https://doi.org/10.1039/c7sm00315c
15. Sing CE, Zwanikken JW, Olvera de la Cruz M (2014) Electrostatic control of block copolymer morphology. Nature Material 13:694–698. https://doi.org/10.1038/NMAT4001
16. Lai J-Y, Lin S-F, Lin F-C, Wang D-M (1998) Construction of ternary phase diagrams in nonsolvent/solvent/PMMA systems. J Polym Sci 36:607–615. https://doi.org/10.1002/(SICI)1099-0488(199803)36:4<607::AID-POLB7>3.0.CO;2-L
17. Zhang W, He J, Bao H, Dong X (2015) Polymeric Janus nanoparticles from triblock terpolymer micellar dimers. RSC Adv 5:104223–104227. https://doi.org/10.1039/c5ra17384a
18. Jafari M (2018) Application of Hansen solubility parameters in fabrication of molecularly imprinted polymers for detection of PAHs from water samples. M.Sc. thesis, Memorial University of Newfoundland and Labrador, Canada
19. Ibraeva ZE, Hahn M, Jaeger W, Bimendina LA, Kudaibergenov SE (2004) Solution Properties and Complexation of Polyampholytes based onN,N-Dimethyldiallylammonium Chloride and Maleic Acid or Alkyl (Aryl) Derivatives of Maleamic Acids. Macromol Chem Phys 205:2464–2472. https://doi.org/10.1002/macp.200400242
20. Tsitsilianis C, Aubry T, Iliopoulos I, Norvez S (2010) Effect of DMF on the rheological properties of telechelic polyelectrolyte hydrogels. Macromolecules 43:7779–7784. https://doi.org/10.1021/ma101238s
21. Tsitsilianis C, Stavrouli N, Bocharova V, Angelopoulos S, Kiriy A, Katsampas I, Stamm M (2008) Stimuli responsive associative polyampholytes based on ABCBA pentablock terpolymer architecture. Polymer 49:2996–3006. https://doi.org/10.1016/j.polymer.2008.04.058
22. Vidulich GA, Evans DF, Kay RL (1967) The dielectric constant of water and heavy water between 0 and 40. Degree. J Phys Chem 71:656–662. https://doi.org/10.1021/j100862a028
23. O'Neil MJ, Heckelman PE, Koch CB, Roman KJ (2006) The Merck Index, an Encyclopedia of Chemicals, Drugs, and Biologicals. 14th edn. Merck Co., Inc., Whitehouse Station, NJ
24. Feoktystov AV, Frielinghaus H, Di Z, Jaksch S, Pipich V, Appavou M-S, Babcock E, Hanslik R, Engels R, Kemmerling G, Kleines H, Ioffe A, Richter D, Brückel T (2015) KWS-1 high-resolution small-angle neutron scattering instrument at JCNS: current state. J Applied Crystallogr 48:61–70. https://doi.org/10.1107/S1600576714025977
25. Heinz Maier-Leibnitz Zentrum et al. (2015) KWS-1: Small-angle scattering diffractometer. Journal of Large-Scale Research Facilities 1(1–4):A28. https://doi.org/10.17815/jlsrf-1-26
26. Porod G (1951) Die Röntgenkleinwinkelstreuung von dichtgepackten kolloiden Systemen. Kolloid-Z. 123:83–114. https://doi.org/10.1007/BF01512792
27. Schmidt PW (1982) Interpretation of small-angle scattering curves proportional to a negative power of the scattering vector. J Appl Crystallogr 15:567–569. https://doi.org/10.1107/S002188988201259X
28. Guinier A, Fournet G (1955) Small-angle scattering of X-rays. John Wiley and Sons Inc., New York
29. Neutron activation and scattering calculator, https://www.ncnr.nist.gov/resources/activation/, accessed July 15, 2020
30. Kotlarchyk M, Chen S-H (1983) Analysis of small angle neutron scattering spectra from polydisperse interacting colloids. J Chem Phys 79:2461–2469. https://doi.org/10.1063/1.446055
31. Schulz GV (1935) Über die Kinetik der Kettenpolymerisationen. Z Phys Chem 43:25–46
32. Percus JK, Yevick GJ (1958) Analysis of classical statistical mechanics by means of collective coordinates. Phys Rev 110:1–13. https://doi.org/10.1103/PhysRev.110.1
33. http://www.sasview.org/ (accessed April 10, 2020)
34. Halperin A, Alexander S (1989) Polymeric micelles: their relaxation kinetics. Macromolecules 22:2403–2412. https://doi.org/10.1021/ma00195a069
35. Ma Y, Lodge TP (2016) Chain exchange kinetics in diblock copolymer micelles in ionic liquids: the role of χ. Macromolecules 49:9542–9552. https://doi.org/10.1021/acs.macromol6b02212
36. Wang E, Zhu J, Zhao D, Xie S, Bates FS, Lodge TP (2020) Effect of solvent selectivity on chain exchange kinetics in block copolymer micelles. Macromolecules 53:417–426. https://doi.org/10.1021/acs.macromol9b01877

Margarita A. Dyakonova studied chemistry at Novosibirsk State University where she graduated in 2010. She did her master studies in the area of material science at Rennes University, France, and her master and PhD thesis in the group of Prof. Christine M. Papadakis, where she investigated the behavior of stimuli-responsive polymers. Afterwards, she has continued working in the material engineering field.

Yanan Li studied material science and got her master degree in 2019 at Beijing University of Chemical Technology of China on the preparation of porous materials from emulsions. Since then, she has been a Ph.D. student in the group of Christine M. Papadakis, where she investigates multiresponsive polymer micelles by scattering methods, also at large facilities.

Ioanna N. Besiri is a Chemical Engineer, graduated with the Diploma degree from Technical University of Patras, in 2018. Now, she is a Ph.D. student at Technical University of Munich in the School of Life Sciences Weihenstephan. She has been working on the rheological behavior of polymers for five years. Specifically, her diploma thesis was focused on the rheological characterization of responsive physical hydrogels from telechelic polyampholytes. In her doctoral studies, she investigates the in situ rheological behavior of crosslinking systems using a custom-made rheological setup.

Zhenyu Di did his Ph.D. work with Christine M. Papadakis and graduated in 2010. From 2010 to 2016, he was the second instrument responsible and local contact for the SANS instrument KWS-1 at the Jülich Centre for Neutron Science (JCNS) at the Heinz Maier-Leibnitz-Zentrum in Garching, Germany. His research focused on block copolymer blends and morphology of microemulsions under shear.

Isabelle Grillo did her PhD at the CEA in Saclay, France, in 1998. She joined the Large Scale Structures Group at the Institut Laue-Langevin (ILL) in Grenoble, France, in 1998. She became co-responsible for the small-angle neutron scattering (SANS) instrument D22 for 5 years, then responsible for the ILL chemistry labs for 9 years, while continuing to serve as a local contact for the SANS instruments. Finally, she returned as an instrument responsible for the SANS instrument D33 in 2012. Her scientific interests lied in the field of surfactants, nanoparticles, polymers and emulsion droplets, as seen through small-angle scattering. Isabelle sadly passed away in 2019. We dedicate this paper to her.

Constantinos Tsitsilianis received his Ph. D. in physical chemistry of polymers from the Department of Chemical Engineering at the University of Patras. He did his postdoctoral research on polymer chemistry in the institute "Charles Sadron" in Strasburg. He was appointed as full Professor in the Department of Chemical Engineering at the University of Patras in 2005. He was Invited Professor at the Université Pierre et Marie Curie, E.S.P.C.I. in Paris (1998), in Matière Molle et Chimie, ESPCI-ParisTech, (2010) and at Département Polymères, Colloides et Interfaces, Université du Maine, Le Mans, France (2017). His research interest is in the area of macromolecular engineering, comprising synthesis and characterization of model macromolecules via controlled polymerization methods, polymer self-assemblies comprising nano-structured micelles and reversible physical hydrogels from stimuli responsive model block copolymers. He is co-author of more than 130 peer-reviewed scientific articles, and 10 chapters in books.

Christine M. Papadakis received her Ph.D. degree at Roskilde University, Denmark in 1996. After a postdoctoral stay at Risø National Laboratory in Denmark, she did her habilitation at the University of Leipzig. In 2003, she was appointed Associate Professor for Experimental Physics/Soft Matter at TUM. Her research interests cover amphiphilic and (multi)responsive polymer systems, polymers under high pressure, polymers for medical applications, and block copolymer thin films, including in situ and kinetic scattering methods, also at large facilities. She is co-author of more than 150 peer-reviewed scientific articles. She is one of the Editors-in-Chief of Colloid and Polymer Science.